Effect of partial substitution of highly reactive mineral additions by nanosilica in cement pastes

João Henrique da Silva Rêgo[a*], Moisés Frías Rojas[b], Amparo Moragues Terrades [c], Lucía Fernández-Carrasco[d], Enrique Romero Morales[e], Maria Isabel Sánchez de Rojas[f]

[a] D.Sc. Postgraduate Program in Structural Engineering and Construction, University of Brasília, Campus Universitário Darcy Ribeiro, 70910-900, Brasília - DF, Brazil.

[b] D. Sc. Eduardo Torroja Institute for Construction Science (IETcc-CSIC), C/Serrano Galvache, 4, 28033, Madrid, Spain.

[c] D.Sc. Higher Technical School of Road, Channel and Port Engineers, Polytechnic University of Madrid, C / Profesor Aranguren s / n. Ciudad Universitaria, 28040, Madrid, Spain.

[d] D.Sc. Higher Technical School of Road, Channel and Port Engineers, Polytechnic University of Catalonia. C / Jordi Girona 1-3, 08034, Barcelona, Spain.

[e] D.Sc. Higher Technical School of Road, Channel and Port Engineers, Polytechnic University of Catalonia. C / Jordi Girona 1-3, 08034, Barcelona, Spain.

[f] D. Sc. Eduardo Torroja Institute for Construction Science (IETcc-CSIC), C/Serrano Galvache, 4, 28033, Madrid, Spain.

*Corresponding author.

E-mail address:*jhenriquerego@ig.com.br*

Abstract

The phenomena involved in portland cement hydration and interactions with nanosilica are very complex and not yet fully understood. In addition, few papers have currently proposed to investigate the microstructure and mechanical properties of ternary mixtures using portland cement, colloidal nanosilica, and highly reactive mineral additions. This article investigates, for the first time, the behavior of different highly reactive mineral additions (silica fume and metakaolin) when partially replaced by colloidal nanosilica in the microstructure and hydration of cementitious materials. For the study of the cementitious material microstructures, a Langavant calorimeter, compressive strength, X-ray diffraction, thermogravimetry, infrared spectroscopy, and mercury intrusion porosimetry were used. The pastes with a 1% substitution of highly reactive mineral additions by nanosilica showed higher compressive strength and more refined porosity than the pastes with only silica fume or metakaolin. The results show that nanosilica appears to have better synergism with metakaolin than with silica fume.

Keywords: *Nanosilica, silica fume, metakaolin, blended cements, microstructure, properties.*

Introduction

Some materials such as silica fume and metakaolin are classified as highly reactive mineral additions because of their high pozzolanic reactivity and are used for the production of high-performance cementitious materials. Silica fume was the first highly reactive mineral addition used to produce high strength concrete (Mehta and Monteiro 2014). It has a high content of amorphous silica in its composition, which, by the pozzolanic reaction, interacts with the calcium hydroxide coming from the hydration reaction of the cement, generating secondary C-S-H gels. In addition, it reduces the overall Ca/Si ratio, increases the mean chain length and alters the C-S-H morphology (Rossen et al. 2015). The high fineness of its particles also contributes to the physical action (filler effect) by refining the pores and decreasing the total porosity of the cementitious materials (Juenger and Siddique 2015).

Metakaolin has been increasingly studied in recent years and several articles have demonstrated the elevated potential for high performance concrete production (Juenger and Siddique 2015, Frías et al. 2015). It has a high content of alumina in its composition, which differentiates it from the silica fume that presents its composition constituted mainly of silica. In the pozzolanic reaction of metakaolin, the C-A-S-H formation occurs with the substitution of part of the silicon by aluminum in the C-S-H chains (Lothenback et al. 2011). The inclusion of Al in the C-S-H chain generates more polymerized gels and with longer chains (Torres et al. 2015).

In recent years, the availability of nanoparticles has made possible great strides in material science and technology. The incorporation of nanoparticles into new materials provides changes in their microstructure, influencing the physical, mechanical and chemical properties and reflecting in their performance. Among the nanoparticles used in cementitious materials, the nanosilica stands out. The nanoparticles of silica (nanosilica)

have superior reactivity when compared to the particles of the same chemical composition and of larger size, such as the silica fume (Puentes et al. 2015; Nili et al. 2015; Singh et al. 2015a; Chen et al. 2016, Alonso-Rodriguez et al. 2017), as well as accelerate cement hydration reactions (Singh et al. 2015a, Singh et al. 2015b, Hou et al. 2015, Singh et al. 2016, Moon et al. 2016). The C-S-H formed is more polymerized and has longer chains (Singh et al. 2015, Moon et al. 2016). Thus, nanoscale grains participate more effectively in pozzolanic reaction, resulting in new materials with higher performance than the same materials without the use of nanoparticles. Although the potential of nanosilica to provide increased strength of cementitious materials is evident, there is no consensus as to the best percentage and under which mixing conditions the best performance can be obtained (Senff 2009; Sanchez and Sobolev 2010; Alonso-Dominguez et al. 2012; Kong et al. 2013; Ahari et al. 2015).

A few papers have been proposed to investigate the microstructure and mechanical properties of ternary mixtures using Portland cement, colloidal nanosilica and highly reactive mineral additions. Some researchers such as Amim et al. 2015, Jalal et al. 2015, Nili and Ashan 2015, Khaloo et al. 2016, Gesoglu et al. 2016, and Garg et al. 2016, reported the beneficial effect on the mechanical properties and microstructure of cementitious materials with the simultaneous incorporation of silica fume and nanosilica. Only one research that evaluates the joint effect of metakaolin and nanosilica incorporation in cement pastes was found (Andrade et al. 2018).

One of the current trends in nanotechnology studies is to understand the interaction between nanomaterials and their base materials and, in the case of nanosilica, to deepen the understanding of the modification in C-S-H caused by its incorporation (Lazaro et al. 2016). Thus, it is essential to continue the existing studies, aiming at a better

understanding of the aspects related to the microstructure and properties of cementitious materials with nanosilica and the different types of highly reactive mineral additions.

The present article investigates the microstructure and mechanical properties of Portland cement pastes with the partial substitution of two types of highly reactive mineral additions (silica fume and metakaolin) by the colloidal nanosilica. The characterization of new cement matrices by mean of compression strength, Langavant calorimeter, X-ray diffraction (XDR), thermogravimetric analysis (TGA), infrared spectroscopy (FTIR) and mercury intrusion porosimetry (MIP) were carried out to verify the behavior of different highly reactive mineral additions (silica fume and metakaolin) when partially substituted by the colloidal nanosilica in the microstructure and hydration of the cement pastes.

Experimental program

Materials

The following materials were used in this experimental campaign:

- Cement type V (CPV), following the Brazilian technical standards (NBR 5733 1991), supplied by CIPLAN;
- Nanosilica (NS), based on an aqueous suspension of SiO_2 nanoparticles (30% of solid content), supplied by Akzonobel;
- Metakaolin (MK), supplied by Metacaulim do Brasil;
- Commercial non-densified Silica Fume (SF) supplied by Dow Corning Silicon of Brazil;
- Superplasticizer (SP) based on a polycarboxylate solution (40% of solid content), supplied by Sika.

105 Table 1 and 2 presents the physical and mechanical properties of the cement and
106 chemical compositions of starting materials (cement, SF, MK and NS), determined by X-
107 ray fluorescence spectrometry. The specific surface area values (BET) and water soluble
108 alkalis are also included. As observed in Table 2, MK contains 57% of silica and 32% of
109 alumina, while SF contains 94% of silica. This different content has an influence on the
110 hydration process of the cement pastes with MK or SF. The NS was composed mainly by
111 silica (89%). It is important to note that the loss on ignition was determined with the solid
112 residue of the NS, previously dried at 100ºC.
113 Figure 1 shows XRD patterns of starting materials. The peaks presented in the
114 MK diffractogram (Figure 1a) indicate that the kaolinite did not undergo complete
115 transformation into metakaolin, possibly due to activation temperatures below 600°C.
116 Although the presence of kaolinite peaks in the X-ray diffractogram has been evidenced,
117 there is an weak amorphous halo corresponding to the baseline deviation between the
118 angles of 15 and 30 degrees (2θ), indicating the amorphousness of the material. The
119 diffractogram of SF did not show peaks of crystalline materials identified, i.e., it is
120 completely amorphous. The diffractogram of colloidal NS showed amorphous halo
121 between 15 and 30º, and small peaks that characterize possible crystalline phases of the
122 silica oxide (quartz and cristobalite at 27º and 36º, respectively). Figure 1b shows the
123 crystalline mineralogical phases present in the CPV cement, which is formed by the
124 anhydrous phases (C_3S and C_2S mainly), calcite and traces of quartz.
125 The granulometric distribution of SF and MK by laser granulometry is shown in
126 Figure 2. The laser granulometry test was performed as described in (EDANA 2002). The
127 laser granulometer - CILAS - Microcurve Model was used. When analyzing the
128 granulometric distribution of SF, a mean diameter of 36.27 μm, D_{10} = 7.58 μm and D_{90} =

64.86 µm was observed; while for the MK was of 18.70 µm, 2.48 µm and 39.88 µm respectively.

Figure 3 shows SEM images of MK and SF, being: Figure 3a: MK (x300), Figure 3b: MK (x2500), Figure 3c: SF (x300) and Figure 3d: SF (x2500). The analyses were performed in a Scanning Electron Microscope (SEM) Jeol, model JSM-IT300. It was observed that SF presented larger particle sizes when compared to MK. The MK seems to have greater variation of particle sizes, whereas the SF presents particles of more homogeneous sizes (Fig. 3c). When the magnification of the microphotography increased (x2500) (Fig. 3d), the formation of clusters formed by smaller particles of SF was observed. MK appears to be composed of individual grains that have some smaller particles on their surface.

Figure 4 shows TEM images of NS, where spherical SiO_2 nanoparticles, measuring around 27nm in diameter, may be observed. Due to their high surface energy, interparticle distance and molecular configuration, these nanoparticles tend to form clusters (Seekkurachchi, 2008).

Composition and preparation of cement pastes and mortars

Five pastes were produced with Portland cement CP V, SF or MK with/without NS and their compositions are presented in Table 3. The pastes were produced with a fixed water/binder (w/b) ratio equal to 0.35. In order to do that, the water contents from NS and SP were deducted from the total amount of water used to prepare the pastes. The content of 10% of cement replacement by the mineral additions was selected as the maximum value indicated by European standards for SF (AENOR UNE-EN 197-1 2011).

The blended cement mortars were tested with Langavant calorimeter, elaborated according to the requirements described in European standards (UNE - EN 196-5 2011) with a w/b ratio of 0.48.

The mini-slump test was used based on Kantro 1980, which allows the consistency of the fresh pastes to be compared between different formulations. The w/b ratio was set at 0.35 in the pastes and suitable percentages of polycarboxylate superplasticizer additive were added in order to maintain the consistency 94 ± 4 mm for all pastes. This consistency was considered the most favorable for the mixing and molding processes. The consistency of the pastes was measured by the mini slump test, repeated 3 times for each formulation.

The pastes were produced in a climatic room at the temperature of 23 ± 1ºC, using a universal mortar mixing machine, following the requirements of NBR 13276 2005. The procedure to prepare the pastes consisted in adding the water/SP/NS mix to the cement/SF mix or MK and homogenizing the resulting paste for 60s at 140rpm and, then, for 90s at 280rpm. Soon after mixing, cylindrical specimens of 50 x 100 mm were manufactured. After preparation, the molds were kept in a humid chamber for 24h; later they were demolded and kept at the same curing conditions until the compression tests were performed.

The samples employed for the XRD, TGA and FTIR tests were obtained from the center of the specimen used for the compression test. The hydration reaction was stopped by immersion in isopropanol during 24 hours and drying at 40ºC for 24h. Afterward, they were crushed and ground in an agate mortar until reaching a fineness below 75µm. Soon after the cement pastes milling, the samples were packed in plastic film and placed in a hermetically sealed environment in the presence of silica gel, to avoid the presence of moisture, and soda lime to avoid carbonation.

One cube measuring 1cm^3 was extracted from the center of an intact paste cylinder using a diamond cutter and destined to the MIP test. Its hydration was stopped by the same procedure used to prepare the samples for the XRD, TGA and FTIR tests.

Instrumental techniques

The Langavant calorimeter (UNE - En 196-5 2011) measured the heat of hydration of the mortars produced with the 5 pastes analyzed during the first 48 hours of hydration. The compressive strength test of the pastes was performed on days 2 and 28 and was based on NBR 7215 1997 with adaptations to use w/b ratio = 0.35 in pastes. X-ray diffraction and thermogravimetric (TG) analysis were performed on pastes on days 2 and 28 of hydration. Mercury intrusion porosimetry and infrared spectroscopy were performed in the pastes at 28 days of hydration.

The compressive strength of pastes was obtained from direct compression tests of three cylindrical specimens measuring 50 mm in diameter and 100 mm in length. The results presented are the average of the compressive strength of the 3 specimens. Tests were performed in a universal test machine at a pressure application rate equal to 0.25 ± 0.05 MPa/s according to NBR 7215 1997. TGA was performed from 30 to 1000ºC at a heating rate of 10ºC/min with N_2 flow of 100mL/min using a SDT Q-600 thermobalance. In each analysis, approximately 10mg of paste were tested in 90µL alumina crucibles. XRD was performed in a BRUKER D8 Advance powder diffractometer in reflection Bragg-Brentano geometry equipped with a Cu detector (active length of 2θ) and a fixed divergence slit of 0.20º. It operates with Ni-filtered CuKα radiation (λ = 1.5406 Å) at 40 kV and 40 mA. Diffraction patterns were recorded from 5º2θ to 60º2θ at the velocity of 1.2º2θ/min. FT-IR was conducted from 4000 to 400cm^{-1} using KBr pellets at a cement paste/KBr ratio equal to 1/3. The equipment used was a Mattson genesis II spectrometer.

Total porosity and pore-size distribution were determined in cement pastes using a Micromeritics Autopore IV 9500 mercury intrusion porosimeter at a pressure of 227.5MPa. The mercury contact angle used in this study was 141.3º, with a mercury surface tension of 485 dyne/cm^2.

Results and discussion

Fresh state - superplasticizer consumption in the pastes

The SP dosage was adjusted in each paste to produce the consistency of 94mm ± 4mm. The results obtained are shown in Figure 5. Pastes having 10% SF or MK required more SP than the reference paste to achieve the required consistency. This behavior was expected since the mineral additions have a high specific surface, which demand greater amount of water for proper grain wetting. As a result of the increase in the content of MK, SF or NS, there is a tendency to increase the SP content in the pastes, being the most pronounced effect for NS (Chen et al., 2016, Barbhuiya et al. 2015). With the substitution of 1% of the mineral additions by NS, an increase of the SP content was observed in relation to the binary mixtures.

XRD

It was not possible to observe a significant change in the $Ca(OH)_2$ peaks in the pastes at 2 days in relation to the reference paste. At 28 days, it was verified that the pastes incorporating SF and MK with and without NS presented a reduction of the $Ca(OH)_2$ peak in relation to the reference, as can be observed in Figure 6. In all pastes with incorporation of MK, the peak related to kaolinite that appears as impurity due to inefficient combustion

of clay was observed. In all of the pastes, the characteristic peaks of quartz and calcite appear as impurities in the CP V cement. The intensity of the quartz peak increased in the pastes with MK that also presents this impurity. A reduction in the height of the characteristic peaks of the anhydrous calcium silicate phases (C_2S and C_3S) was detected in all the pastes in comparison with the reference paste. This behavior is expected since there is less clinker in these pastes, but it may also be motivated by the greater hydration of cement pastes by the nucleation points effect related to the fineness of mineral additions.

TGA

The calcium hydroxide contents of all pastes were obtained from the TG/DTG curves, as shown in Figure 7 for the CPV paste with w/binder ratio of 0.35 subjected to 2 days of hydration. The portlandite amount (T.CH) was quantified by the mass loss (H_2O) in the temperature range from 450ºC to 550ºC. The portlandite index (I.CH) corresponds to the ratio between the portlandite content of any paste and the portlandite amount quantified in the reference paste at the same age. The results obtained by TGA analysis of the pastes on days 2 and 28 of curing are present in Table 4.

In the paste 100% CPV, an increase of the T.CH along the hydration was observed, indicating the progress of the hydration reaction of cement particles from 2 to 28 days. The pastes 10SF and 10MK showed a reduction of the T.CH in relation to the reference, in part due to the lower amount of cement incorporated in these blended pastes and part of the pozzolanic reaction. When the 1% substitution of the mineral additions by NS occurs, the reduction of T.CH was more pronounced at both days 2 and 28, due to its greater pozzolanic activity and fineness (80.000 m^2/kg).

246 The I.CH in the pastes 10SF and 10MK decreases with increasing hydration age,
247 presenting values of 80.26% and 85.85%, respectively, at 2 days and reaching 72.70%
248 and 70.74 % at 28 days. This indicates that the pozzolanic reaction of these additions
249 occurs in greater intensity after 2 days. In the pastes with 1% substitution of the mineral
250 additions by the NS, a strong reduction of the I.CH up to 2 days with respect to the
251 reference was observed. At 28 days, a reduction of I.CH was more pronounced as a
252 consequence of the pozzolanic reaction of the SF and the MK. The pastes 9SF 1NS and
253 9MK 1NS, being formed by a mixture of pozzolans with different reaction rates, the final
254 pozzolanic reaction would be a synergy of 2 different reactions as the first result of
255 pozzolan NS, followed by the reaction of SF or MK. This behavior was observed in pastes
256 with partial replacement of the cement by MK and NS (Andrade et al. 2018).

257

258 ***FTIR***

259 FTIR was employed to analyze the hydration products in blended pastes
260 containing SF or MK and NS at the age of 28 days. Figure 8 shows the frequency range
261 between 700 and 1300 cm^{-1} for all the pastes analyzed.

262 According to Torres et al. 2014, the peak observed around 975 cm^{-1} corresponds
263 to vibrations of Si-O bonds present in middle-chain tetrahedral (Q_2) in the C-S-H. The
264 relative intensity of the peak 975 cm^{-1} is lower in the reference paste than in the other
265 pastes. The 10SF and 10MK pastes showed peaks in the C-S-H region slightly larger than
266 the reference. When 1% of the mineral additions are replaced by NS, an increase in the
267 characteristic peak of C-S-H is observed, and this effect is more pronounced for MK. This
268 indicates the in these pastes there is an increase in the presence of Si-O bonds present in
269 middle-chain tetrahedral (Q_2) in the C-S-H with consequent increase in the length of its
270 chain. It is important to note that a better synergy occurs in the pastes with MK and NS

than in the pastes with SF and NS. According to Peres et al. 2014, the use of NS promotes the incorporation of Al within the structure of C-S-H. The C-S-H gel formed in these pastes is due to both the C-S-H formed by the hydration of the cement and also the C-S-H formed by the pozzolanic reaction (Andrade et al. 2018).

The peak observed around 860cm^{-1} is characteristic of carbonate ion (Vasquez-Moreno and Blanco-Varella, 1981). The CPV cement can contain up to 5% limestone filer ($CaCO_3$ - calcite) in its composition which justifies of carbonate ion presence in the cement pastes. The observed peak around 1120 cm^{-1} is characteristic of the hydrated aluminate phases (Guerrero et al. 2014). That peak around 1120 cm^{-1} in the pastes 10SF and 10MK have a height very close to the reference peak. In the case of the paste 9SF 1NS, as the formation of the aluminate phases depends only on the hydration of the cement, the substitution of 1% of the SF by the NS increased the hydration degree of the cement. In the case of the paste 9MK 1NS, in addition to increasing the hydration of the cement, MK can contribute with more aluminate phases in the system, generating higher peaks of the hydrated aluminate phases.

The results indicate an increase of C-S-H chain length in the pastes 9SF 1NS and 9MK 1NS, both due to the pozzolanic reaction of the NS and the mineral additions as well as to the increase of the hydration degree of the portland cement.

Langavant Calorimeter in mortars

The Langavant method measures the heat of hydration of the mortar cements by means of a semi-adiabatic calorimeter. Thus, the effect of the substitution of SF, MK and SF or MK together with NS in relation to cement in the hydration of the mortars of the

295 analyzed binders can be verified. The effect of the 1% substitution of the highly reactive
296 mineral additions by NS on the temperature of the mortars is illustrated in Figure 9. The
297 maximum temperatures in all mortars were reached between 15 and 20 h, depending on
298 the cement analyzed. The maximum temperature of the mortar CPV (reference) was of
299 36.5ºC at 18 h. Mortar 10SF showed a maximum temperature similar to the reference
300 (36.7°C) but at 20 h of hydration. Mortar 9SF 1NS showed maximum temperature similar
301 to the reference and development of temperature very close to the reference until the 30
302 hours and then a reduction of temperature. Mortar 10MK showed a reduction of the
303 maximum temperature (35.7ºC) and lower temperature for all ages in relation to the
304 reference. The mortar 9MK 1NS presented the highest maximum temperature (37.9 ºC)
305 and it was reached faster for in relation to all the mortars (15 h). The substitution of 1%
306 of MK by NS accelerates the hydration reactions of the cement with MK up to 15 h.

307 Figure 10 illustrates the effect of the replacement of SF or MK by 1% of NS in
308 the heat of hydration. The reference mortar tended to stabilize the heat of hydration at 41
309 h. The mortar 10SF presented a similar behavior with respect to the reference mortar. In
310 the mortar 9SF 1NS, there was a tendency to stabilize at 41 hours with a value of 322 J/g.
311 The mortars made with MK show a different calorimetric evolution than the other
312 mortars analyzed, mainly with the addition of 1% of NS. The paste 10MK experienced
313 an increase in the heat of hydration from the 14 h of reaction. This same tendency was
314 also observed by Frías et al (2000) working with 10% MK blended cement mortars.
315 The replacement of 1% MK by 1% NS in the mortars 9MK 1NS produced a
316 significant increase in the heat of hydration for all ages with tendency to stabilize after 32
317 h. This fact, together with the higher production of the aluminate phases found by the
318 FTIR test, is indicating the acceleration of hydration reaction of ternary MK-NS cements.

319 This behavior corroborates the better synergy between MK and NS than between SF and
320 NS.
321

322 ***Compressive strength***

323 The results of compressive strength (f_c) of all the pastes at the ages of 2 and 28
324 days are the average of the compressive strength of 3 specimens 50mm x 100mm. The
325 performance index (P.I.) corresponds to the ratio between the compressive strength of
326 any paste (f_cB) and the compressive strength obtained in the reference paste at the same
327 age (f_cA), according to equation 1.
328

329 $$P.I. = \frac{fcB}{fcA} x100 \qquad \text{Equation (1)}$$

330 After collecting the experimental results, statistical analysis (ANOVA) was executed on
331 the data of compressive strength and the Duncan test was used to separate the variables
332 applied to the study into homogeneous groups, grouping statistically similar averages and
333 separating the different averages. All the data are presented in Table 5.
334 According to the Duncan test, the pastes at 2 days of hydration were grouped into
335 3 groups of compressive strength. In the first group with lower compressive strength, is
336 inserted the 10SF paste. In the second group are included three pastes: CPV, 9SF 1NS
337 and 10MK. In the thirth group, with higher compressive strength, the 9 MK 1NS paste is
338 observed. The substitution of 1% of SF or MK by NS increased the compressive strength
339 of the paste, respectively from 44.25MPa to 47.71MPa and from 47.00MPa to 53.65MPa.
340 This behavior corroborates the very high pozzolanic reactivity of nanosilica with respect
341 to the other pozzolans. NS becomes very important between the first and seventh day of

342 curing, producing a strong increase in the rate of hydration and the amount of hydrated
343 phases (Tobon et al., 2012).

344 According to the Duncan test, the pastes at 28 days of hydration were grouped
345 into 4 groups of compressive strength. In the first group with lower compressive strength,
346 is inserted the CPV paste. In the second group are included two pastes: 10SF and 10MK.
347 In the thirth group is observed the 9SF 1NS paste and the 9MK 1NS paste with the highest
348 compressive strength is isolated in the fourth group. At 28 days, all pastes presented
349 higher compressive strength values than the reference paste, especially pastes made with
350 1% NS.

351 At 2 days of hydration, the paste 10SF showed a low value of P.I. (93.5%)
352 increasing to 115% at 28 days, indicating that the pozzolanic reaction of the SF occurs
353 more strongly after 2 days. According to Zhang et al., 2016, the increase in compressive
354 strength of SF blended cement pastes was higher at more advanced ages. In the case of
355 paste 9SF 1NS, the P.I. at 2 days is higher (101%) than paste 10SF and increased to 121%
356 at 28 days. Other researchers also observed similar behavior, with a higher performance
357 of NS up to 7 days and SF after 7 days when they acted in isolation (Birick et al., 2014,
358 Alonso-Dominguez et al., 2017).

359 At two days of hydration, the paste 10MK had a low P.I. of less than 100. The
360 pozzolanic additions, such as MK and SF, require calcium hydroxide to produce
361 secondary C-S-H, thus depending on the progressive development of Portland cement
362 hydration, which may reduce its effect at early ages (Mlinarik et al. 2013). At 28 days the
363 P.I. increases to 114%, probably by the pozzolanic reaction of MK. This behavior was
364 also observed by Barbuiya et al. 2015. The substitution of MK by 1% of NS provided an
365 increase of P.I. at 2 days from 99.3 to 113.3. The paste 9MK 1NS presented the highest
366 P.I. at 2 days. This is probably due to the pozzolanic reaction of NS and to the accelerating

367 effect of NS on cement hydration (Seekkuarachchi et al., 2008, Sanchez del Bosque et
368 al., 2015, Singh et al., 2016), but also indicate the better synergism between MK and NS.
369 This increase in P.I. was also observed at 28 days.

370 The order of P.I. for the pastes at 28 days was, from largest to smallest, 9MK 1NS,
371 9SF 1NS, 10SF, 10MK and reference. In addition, according to the Duncan test, the 9MK
372 1NS paste appears as an isolated group with greater resistance to compression, both at 2
373 and 28 days. This behavior corroborates the results presented by infrared spectroscopy
374 when analyzing the chain length of C-S-H gel formed in the pastes and the best synergism
375 between MK and NS.

376 ***MIP***

377 Mercury intrusion porosimetry (MIP) was performed to characterize the porosity
378 and the pore size distribution in the pastes with a w/b ratio of 0.35. Figure 11 shows the
379 results of total porosity, pores larger than 50nm and pores smaller than 10nm obtained for
380 the pastes at 28 days of hydration.

381 With the incorporation of the SF to Portland cement, a slight decrease of the total
382 porosity was detected (Zhang et al. 2016, Alonso-Rodriguez et al. 2017), while an
383 increase of porosity was observed with the incorporation of the MK (Frías, 2006). In
384 general, the differences are very small and can be considered very similar to the reference
385 paste. When 1% of the mineral additions was replaced by NS, there is a light increase in
386 total porosity but in the same order of magnitude.

387 However, it is important to note that the incorporation of highly reactive pozzolans
388 such as SF and MK produces a refinement of pore sizes greater than 50 nm (macroporous)
389 in relation to the reference paste. A maximum value around 2% of porosity observed in

all blended cements versus the 3.5% shown by the reference paste. The incorporation of 1% NS showed a similar behavior to the blended cement pastes without nanosilica.

The reduction of the macroporous content is directly related with durability of the cementitious materials, since these pores are responsible for the permeability and penetration of aggressive agents in the cementitious materials (Mehta and Monteiro 2014).

On the other hand, an increase in the pore content in the range below 10 nm is observed, classified by Mindess et al., 2003 as gel pores, with the incorporation of mineral additions, this effect being intensified when the substitution of 1% NS. This behavior evidences the higher chain length of hydrated silicates in these pastes, since this pore size is related to the pores inside the C-S-H lamellae (Singh et al. 2015a, Isfahani et al. 2016).

Conclusions

Based on the results obtained from the experimental program conducted, the following conclusions may be drawn:

- Silica fume is more prone to particle agglomeration than the metakaolin. This leads to the formation of clusters and increases the particle diameter of silica fume analyzed.
- The combined use of NS and highly reactive mineral additions increases the demand for SP in relation to pastes with SF or MK. This is due to the greater specific surface area of NS.
- According to TG and XRD tests, NS has a greater effect on CH consumption up to 2 days of hydration while MK and SF have their most

evident effect after 2 days of hydration. When NS was used together with SF or MK, there is a combined effect between the two additions in the consumption of CH, with high consumption up to 2 days by the pozzolanic reaction of NS and, after 2 days, by the pozzolanic reaction of SF or MK.

- Pastes incorporating NS in conjunction with SF or MK, showed higher length chain of C-S-H than pastes with the isolated incorporation of SF or MK at 28 days, as can be seen from the FTIR test.

- Pastes 9SF 1NS and 9MK 1NS presented higher compressive strength and more refined porosity than the 10SF and 10MK pastes at 28 days, corroborating the results of the XRD, TG and FTIR tests.
- The substitution of 1% of the highly reactive mineral additions by NS acts differently for SF and MK. NS seems to have better synergy with MK than with SF, as can be seen from the Langavant calorimetry tests.

- Results obtained emphasize the high potential of the ternary cement mixes produced with MK or SF and NS for the production of high performance cementitious materials.

Acknowledgements

The authors also acknowledge the support provided by the European Commission, by Marie Curie IRSES Project GREAT (FP7-PEOPLE-2013-IRSES-612665), Addendum to the Framework Agreement for Collaboration between University of Brasilia (UnB-Brazil) and Spanish National Research Council (CSIC-Spain) (ref: 201504001653451013W-2017), and by the Laboratory of Ceramic Materials (LACER)

435 of the Federal University of Rio Grande do Sul (UFRGS-Brasil) for the laser
436 granulometry and specific surface BET tests.

437 References

438

439 Ahari, R. S., Erdem, T. K., Ramyar, K. (2015). "Effect of various supplementary
440 cementitious materials on rheological properties of self-consolidating concrete",
441 *Const. Buil. Mat*., Vol 75 Issue 30. 89 - 98.

442 Alonso-Dominguez, D., Álvarez-Serrano, I., Reyes, E., Moragues, A. (2017). "New
443 mortar fabricated by electrostatic dry deposition of nano and microsilica additions:
444 Enhanced Properties". *Const. Buil. Mat*., Vol 135. 186-192.

445 Alonso-Dominguez, D., Moragues, A., Reyes, E., Álvarez-Serrano, I. Álvarez-
446 Serrano, (2015). "Estudio de la variacion de la estructura del gel C-S-H em materiales
447 base cemento com adiciones de sílice de distinta granulometria". *In: Proc. XIII*
448 *CONPAT*. Lisboa/Portugal. [CD-ROM].

449 Amin, M., Abu, K. (2015). "Effect of using different types of nano materials on
450 mechanical properties of high strength concrete". *Const. Buil. Mat*., Volume 80 Issue
451 1. 116 - 124.

452 Andrade, D. S., Rêgo J. H. S., Morais P. C., Frías, M. (2018). "Chemical and
453 mechanical characterization of ternary cement pastes containing metakaolin and
454 nanosilica". *Constr Buil. Mat*., Vol 159. 18 - 26.

455 ASSOCIAÇÃO BRASILEIRA DE NORMAS TÉCNICAS. (1991). "Cimento
456 Portland de alta resistência inicial. [Initial high strength Portland cement]". *NBR 5733.*
457 Rio de Janeiro. Brasil.

458 ASSOCIAÇÃO BRASILEIRA DE NORMAS TÉCNICAS. (1997). "Cimento
459 Portland - Determinação da resistência à compressão [Portland cement - Determination
460 of compressive strength]". *NBR 7215*. Rio de Janeiro, 1997.
461 ASSOCIAÇÃO BRASILEIRA DE NORMAS TÉCNICAS. (2005). "Argamassa para
462 assentamento e revestimento de paredes e tetos - Preparo da mistura e determinação
463 do índice de consistência. [Mortars applied on walls and ceilings - Determination of
464 the consistence index]". *NBR 13276*. Rio de Janeiro. Brasil.
465 ASTM. (2004). D 4404-84. "Standard test method for determination of pore volume
466 and pore volume distribution of soil and rock by Mercury intrusion porosimetry". *D*
467 *4404-84*.
468 Barbhuiya, S., Choer, P. L., Menon, S. "Microstructure, hydration and
469 nanomechanical properties of concrete containing metacaulim". *Const. Buil. Mat*., Vol
470 95. 696-702.
471 Birick, H., Sarier, M. (2014). "Comparative Study of the Characteristics of nanosilica-
472 silica-fume and fly ash incorporated cement mortars". *Mat. Res.,* Vol 1(3). 370-382.
473 Chen, Y., Deng, Y., Li, M. (2016). "Influence of Nano-SiO2 on the Consistency,
474 Setting Time, Early-Age Strength, and Shrinkage of Composite Cement Pastes". *Adv.*
475 *Mat. Sci. Eng*., Volume 2016, Article ID 5283706, 8 pages.
476 http://dx.doi.org/10.1155/2016/5283706.
477 EDANA – European Disposals and Nonwovens Association. (2002). "Recommended
478 test method: free swell capacity". *ERT 440.2-02.*
479 European Standard EN 196-5 (2011): Methods of testing cement. Part 5: Pozzolanicity
480 test for pozzolanic cement.
481 European standard EN 197-1 (2011): Cement Part 1. Composition, specifications and
482 conformity criteria for common cements.

Frías, M. (2006). “The effect of MK on the reaction products and microporosity in blended cement pastes submitted to long hydration time and high curing temperature”, *Adv.Cem. Res.*, 18 1. 1 - 6.

Frías, M., Rodriguez, O., Sanchez de Rojas, M. I. (2015). “Paper sludge, an environmentally sound alternative source of MK-based cementitious materials: A review”, *Const. Buil. Mat*., Volume 74 15, 37-48.

Frías, M., Sanchez de Rojas, M.I., Cabrera, J. (2000). ”The effect that the pozzolanic reaction of metakaolin has on the heat evolution in metakaolin-cement mortars”, *Cem. Concr. Res.*, Vol 30. 209 - 216.

Garg, R., Bansaland, M., Aggarwal, Y. (2016). “Strength, Rapid Chloride Penetration and Microstructure Study of Cement Mortar Incorporating Micro and Nano Silica”, *Int. J. Electrochem. Sci*., Vol 11. 3697 - 3713.

Gesoglu, M., Gunoisi, E, Assad, D., Fakhraddin, M. (2016). “Properties of low binder ultra-high performance cementitious composites: Comparison of nanosilica and microsilica”, *Const. Buil. Mat*., Volume 101 Issue 15. 706 - 713.

Guerrero, A. M. B., Gaitero, J.J., Quinines, G.P.A., Elizaide, S. G. (2014). “Multi-scale analysis of cement pastes with nanosilica addition”, *Adv. Cem. Res.,* Volume 26. 271 – 280.

Hou, P., Qian, J., Cheng, X., Shah, S.P. (2015). “Effects of the pozzolanic reactivity of nanoSiO_2 on cement-based Materials”. *Cem. Concr. Compos*., Vol 55. 250 - 258.

Isfahani, F.T., Redaelli, E., Lollini, F., Li, W., Bertolini, L., (2016). “Effects of Nanosilica on Compressive Strength and Durability Properties of Concrete with Different Water to Binder Ratios”, *Adv. Mat. Sci. Eng*., Volume 2016, Article ID 8453567, 16 pages. http://dx.doi.org/10.1155/2016/8453567.

Jalal, M. , Pouladkhan, A., Harandi, O .F., Jafari, D. (2015). “Comparative study on effects of Class F fly ash, nano silica and sílica fume on properties of high performance self compacting concrete”, *Const. Buil. Mat*., Volume 94 Issue 30. 90 - 104.

Juenger, M.C.G., Siddique, R. (2015). “Recent advances in understanding the role of supplementary cementitious materials in concrete”, *Cem. Concr. Res.,* Vol 78, 71 - 80.

Kantro, D. (1980). “Influence of Water-Reducing Admixtures on Properties of Cement Paste - A Miniature Slump Test”, *Cem. Concr. Aggr*., Vol. 2 No. 2. 95-102, https://doi.org/10.1520/CCA10190J. ISSN 0149-6123.

Khaloo, M. Mobili, H, Housseini, P. (2016). “Influence of different types of nano-SiO_2 particles on properties of high-performance concrete”, *Const. Buil. Mat*., Volume 113 15.188 - 201.

Kong, D., Young, S., Xiangfei, D., Yang, Y., Shah, S. P. (2013). “Influence of nano-silica agglomeration on fresh properties of cement pastes”. *Const. Buil. Mat*., Vol. 43. 557-562.

Lazaro; Q., Yu, L., Brouwers, H. J. H. B. (2016). “Nanotechnologies for sustainable Construction”. *Book Chapter: Sustainable of Construction Materials.* Http://dx.doi.org/10.1016/B978-0-08-100370-1.00004-4. Elsevier.

Lothenback, B., Scrivener, K., Hooton, R. D. (2011). “Supplementary Cementitious Materials”, *Cem. Concr. Res.*, Vol 41, Issue 12, 1244-1256.

Mehta, P. K., Monteiro, P. J. M. (2014). *Concreto: Estrutura, propriedades e materiais [Concrete: Structure, properties and materials]*, Ibracon, 3ª. Ed., São Paulo, Brasil.

Mindess, S., Francis, J., Darwin, D., (2003). *Concrete*. 2ed. Pearson Education. NJ . USA.

530 Mlinarik, L., Kopecskó, K. (2013). “Impact of metakaolin - a new supplementary
531 material - on the hydration mechanism of cements”, *Acta Tech. Nap.: Civ. Eng. Arch.*.,
532 Vol. 56 2.
533 Moon, J., Redataha, M. M., Youm, K., Kim, J. J. (2016). “Investigation of Pozzolanic
534 Reaction in Nanosilica-Cement Blended Pastes Based on Solid-State Kinetic Models
535 and 29Si MAS NMR”. *Mat*., Vol 9, 99. doi:10.3390/ma9020099.
536 Nili, M., Eshan, A. (2015). “Investigating the effect of the cement paste and transition
537 zone on strength development of concrete containing nanosilica and silica fume”. *Mat.*
538 *Des*., Vol 75 174 - 183.
539 Pérez G., Guerrero A., Gaitero J. J., Goñi S. (2014). “Structural Characterization of C-
540 S-H gel through an improved deconvolution analysis of NMR spectra”, Jour Mater
541 Sci., Vol 49 142 - 152.
542 Puentes, J., Barluenga, G., Palomar, I. (2015). “Effect of silica-based nano and micro
543 additions on SCC at early age and on hardened porosity and permeability.” *Const. Buil.*
544 *Mat.,* 154-161.
545 Rossen, J. E. Lothenback, B. Scrivener, K. L. (2015). “Composition of C-S-H in pastes
546 with increasing levels of silica fume additions”, *Cem. Concr. Res.*, vol. 75, 14 - 22.
547 Sanchez del Bosque, I.F., Martinez-Ramirez, S., Blanco-Varela, M.T. (2015).
548 “Calorimetric study of the early stage of the nanosilica – Tricalcium silicate hydration:
549 Effect of temperature”, *Mat. Const*., Vol. 65, n. 320.
550 Sanchez, F., Sobolev, K. (2010). “Nanotechnology in concrete – A review”, *Const.*
551 *Buil. Mat*., Vol 24 Issue 11. 2060-2071.
552 Seekkuarachchi, I. N., Tanaka, K., Kumazawa, H. (2008). “Dispersion mechanism of
553 nano - particulate aggregates using a high pressure wet - type Jet Mill”, *Chem. Eng.*
554 *Sci*., Volume 63 Issue 9, 2341 - 2366.

555 Senff, L. (2009). “Efeito da adição de micro e nanossílica no comportamento
556 reológico e propriedades no estado endurecido de argamassas e pastas de cimento.
557 [Effect of the addition of micro and nanosilica on rheological behavior and properties
558 in the hardened state of mortar sand cement pastes]”. *[Ph.D thesis]*. Postgraduate
559 Program in Science and Engineering Materials/Federal University of Santa Catarina.
560 Florianópolis, Brasil; 2009.
561 Singh, L. P., Ali, D., Sharma U. (2016). “Studies on optimization of silica
562 nanoparticles dosage in cementitious system”. *Cem. Concr. Comp*., Vol 70. 60 - 68.
563 Singh, L.P., Bhattacharyya, S. K., Mishra, G., Ahalawat, S., Sharma, U. (2015).
564 “Studies on early stage hydration on tricalcium silicate incorporating silica
565 nanoparticles: Part I”. *Const. Buil. Mat*., Vol 74 . 278-286.
566 Singh, L.P., Goel, A. , Battacharyya, S.K., Sharma, U., Mishra, G. (2015). “Hydration
567 studies of cementitious materials using sílica nanoparticles”, *Jour. Adv. Concr. Tech*.,
568 Vol. 13. 345-354.
569 Tobón, J. I., Payá, J. J., Borrachero, M. V., Restrepo, O. J. (2012). “Mineralogical
570 evolution of Portland cement blended with silica nanoparticles and its effect on
571 mechanical strength”, *Const. Bui. Mat*., Volume 36. 736 - 742.
572 Torres, D., Fernandez-Carrasco, L. J., Martinez-Ramirez, S. (2015). “C-S-H gels in
573 Blended Cements: Study by Infrared Spectroscopy”. *In: Proc. 14th International*
574 *Congress on the Chemistry of Cement.* ICCC. Beijing/China. [CD-ROM].
575 Vázquez-Moreno, T., Blanco-Varela, M. T. (1981). Tabla de frecuencias y espectros
576 de absorción infrarroja de compuestos relacionados con la química del cemento. Mat.
577 Constr., Vol *31* 182. 31 - 48.

578 Zang, Z., Zhang, B., Yuyan, P. (2016). “Hydration and microstructures of concrete
579 containing raw or densified silica fume at different curing temperatures”. *Const. Buil.*
580 *Mat*., Vol 121. 483-490.

581 Tables

582

583 Table 1. Properties and characteristics of the cement CP V used in this study.

Setting Time		Blaine	Residue on	Specific mass	Compressive strength (MPa)		
Initial (h:min)	Final (h:min)	(cm^2/g)	sieve #200 (%)	(g/cm^3)	3 day	7 days	28 days
02:17	03:50	3527	1.30	3.09	34.7	41.2	47.9

584

585

586

587 Table 2. Chemical composition of the materials.

Compounds		CP V (%)	SF (%)	MK (%)	NS (%)
Loss on ignition		1.86	3.24	2.89	7.55
Insoluble residue		0.43	-	-	-
Calcium oxide (CaO)		62.5	0.44	0.07	0.02
Silicon dioxide (SiO_2)		19.72	94.17	57.43	89.08
Aluminum oxide (Al_2O_3)		4.54	0.12	32.58	-
Iron oxide (Fe_2O_3)		3.04	0.11	2.08	-
Magnesium oxide (MgO)		5.26	0.68	1.51	0.79
Sulfur trioxide (SO_3)		2.82	0.07	-----	-----
Free calcium oxide (CaO)		0.63	-----	-----	-----
Total Alkali	Sodium Oxide (Na_2O)	0.08	0.24	1.81	0.08
	Potassium oxide (K_2O)	0.59	0.80	-----	0.59
	Na_2O equivalent	0.47	-----	1.81	0.47
Water-soluble alkalis	Sodium oxide (Na_2O)	0.03	-----	0.19	0.03
	Potassium oxide (K_2O)	0.30	-----	-----	0.30
	Na_2O equivalent	0.23	-----	0.19	0.23
Specificy Surface BET(m^2/kg)		-----	19,892	20,143	80,000*

588 *Supplied by the manufacturer

589

590

591 Table 3. Composition of Portland cement pastes.

Pastes	Abbreviation	CPI (g)	Water (g)	SF (g)	MK (g)	NS (g)	SP (g)/(%)	Mini slump (mm)
100% CPV	CP V	1200	416.4	-	-	-	6/0.5	95
90% cement CPV + 10% SF	10SF	1080	413.52	120	-	-	10.8/0.9	98
90% cement CPV + 9% SF + 1%NS	9SF 1NS	1080	382.64	108	-	40	15.6/1.3	91
90% cement CPV + 10% MK	10MK	1080	414.24	-	120	-	9.6/0.8	96
90% cement CPV + 9% MK + 1%NS	9MK 1NS	1080	382.64	-	108	40	15.6/1.3	98

592

593

Table 4. Calcium hydroxide content (T.CH) and Portlandite index (I.CH) of the pastes.

	2days		28days	
Pastes	T.CH (%)	I.CH (%)	T.CH (%)	I.CH (%)
CP V	13.93	100	16.85	100
10SF	11.18	80.26	12.25	72.70
9SF 1NS	10.07	72.29	10.60	62.90
10MK	11.96	85.85	11.92	70.74
9MK 1NS	10.15	72.86	10.69	63.44

Table 5. Compressive strength (fc), Performance index (P.I.) and groups of compressive strength values of the pastes by multiple comparison of averages by Duncan's test at 2 and 28 days of hydration.

Pastes		f_c (MPa)	P.I	Group I	Group II	Group III	Group IV
2 days	CP V	47.33	100.0		x		-
	10SF	44.25	93.5	x			-
	9SF 1NS	47.71	100.8		x		-
	10MK	47.00	99.3		x		-
	9MK 1NS	53.65	113.3			x	-
28 days	CP V	65.61	100.0	x			
	10SF	75.81	115		x		
	9SF 1NS	79.50	121.1			x	
	10MK	74.74	114		x		
	9MK 1NS	86.39	131.7				x

605

606 Figure Captions

607

608 Fig. 1. X-ray diffractograms: a) SF, MK and NS, b) CP V cement.

609 Fig. 2. Particle size distribution of SF and MK.

610 Fig. 3. SEM images a) MK (x300), b) MK (x2500), c) SF (x300), d) SF (x2500).

611 Fig. 4. TEM micrographs of NS.

612 Fig. 5. Superplasticizer content (%) of the pastes to reach the normalized consistency.

613 Fig. 6. X-ray diffractograms of the pastes at 28 days.

614 Fig. 7. TG/DTG curve for the CP V paste w/binder ratio of 0.35 at 2 days of hydration.

615 Fig. 8. FTIR spectra of the pastes: CPV, 10SF, 10MK, 9SF 1NS, 9MK 1NS at 28 days.

616 Fig. 9. Heating over time.

617 Fig. 10. Effect of the different compositions on the heat of hydration of the pastes.

618 Fig. 11. Evolution of porosities in blended pastes after 28 days of hydration.

619

620 Figure 1a

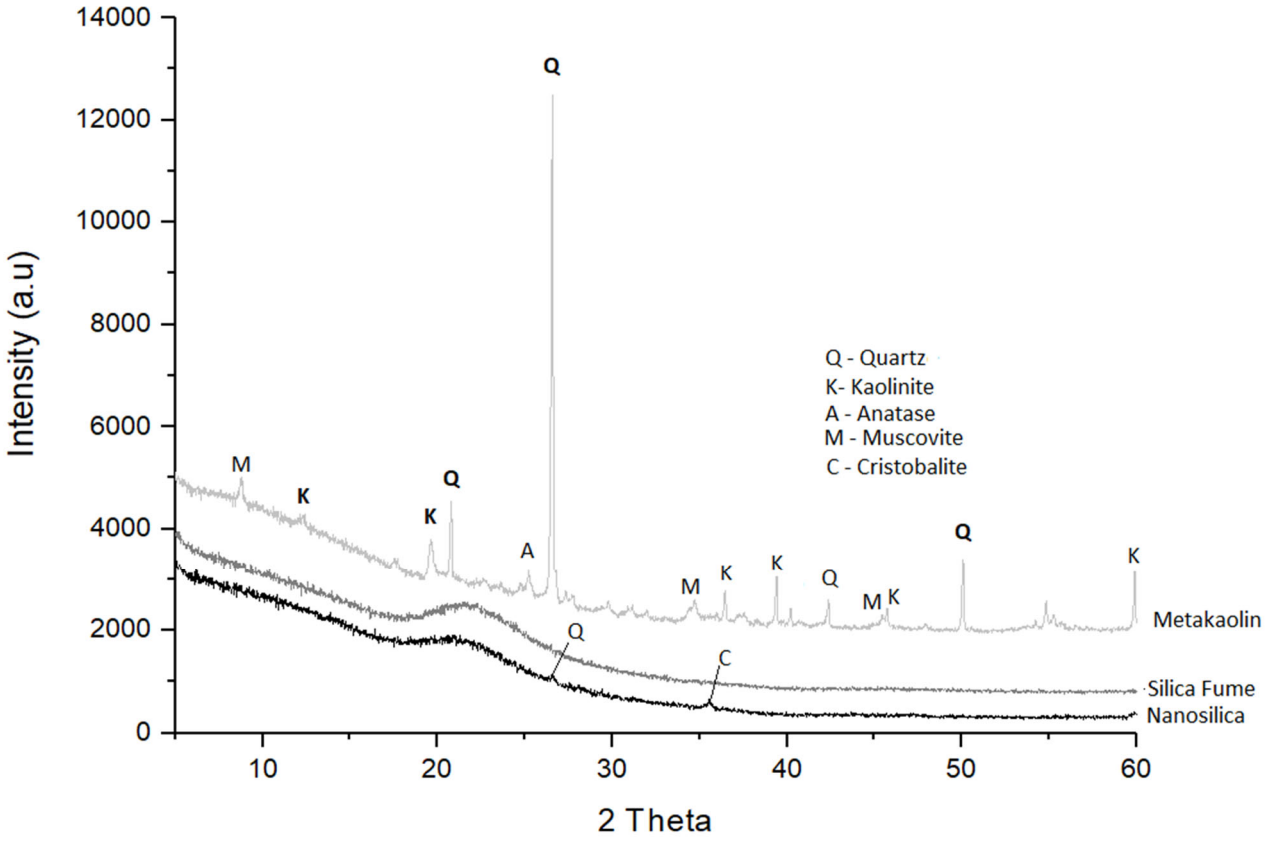

621

622

623 Figure 1b

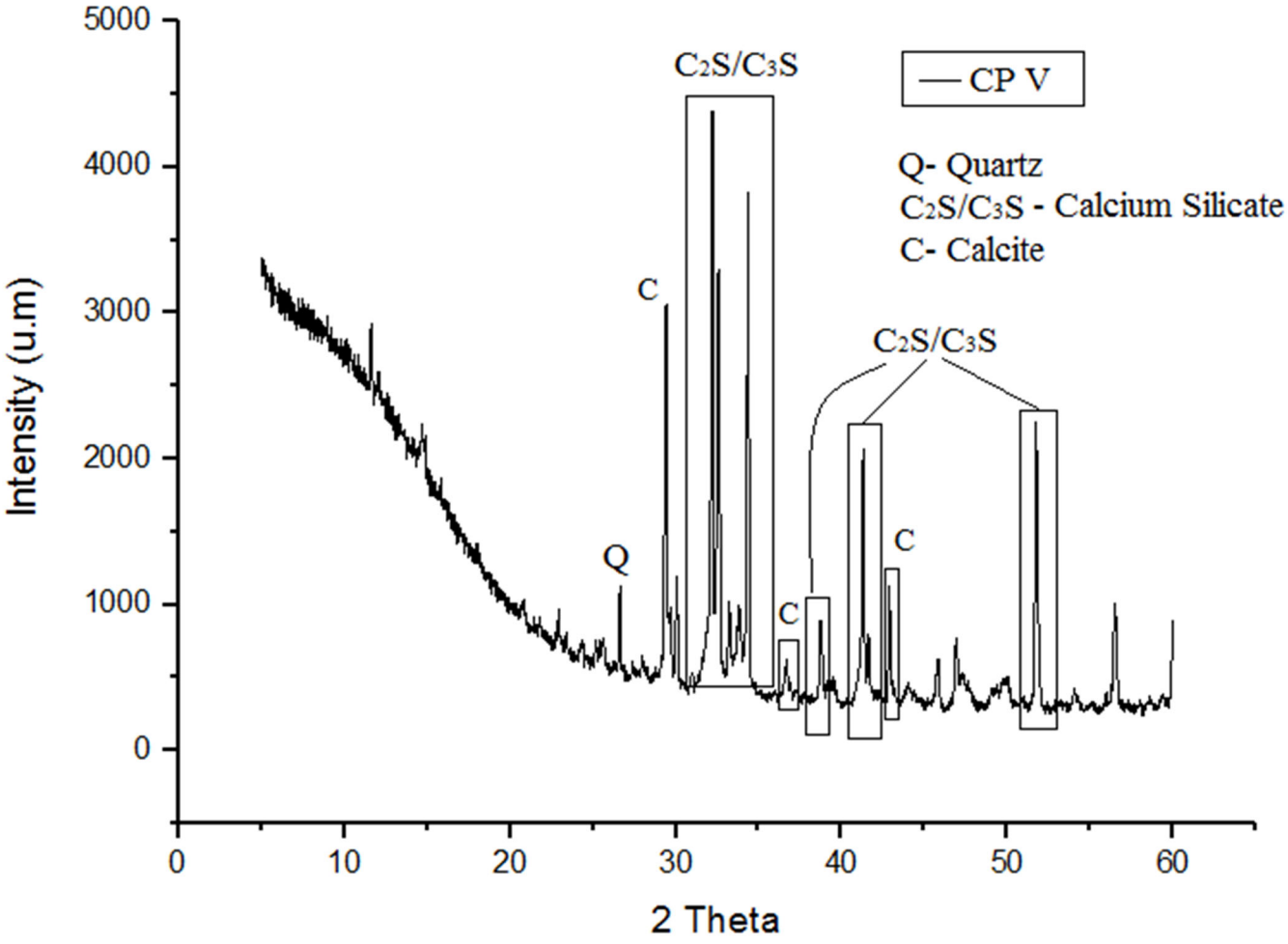

624

625

626 Figure 2

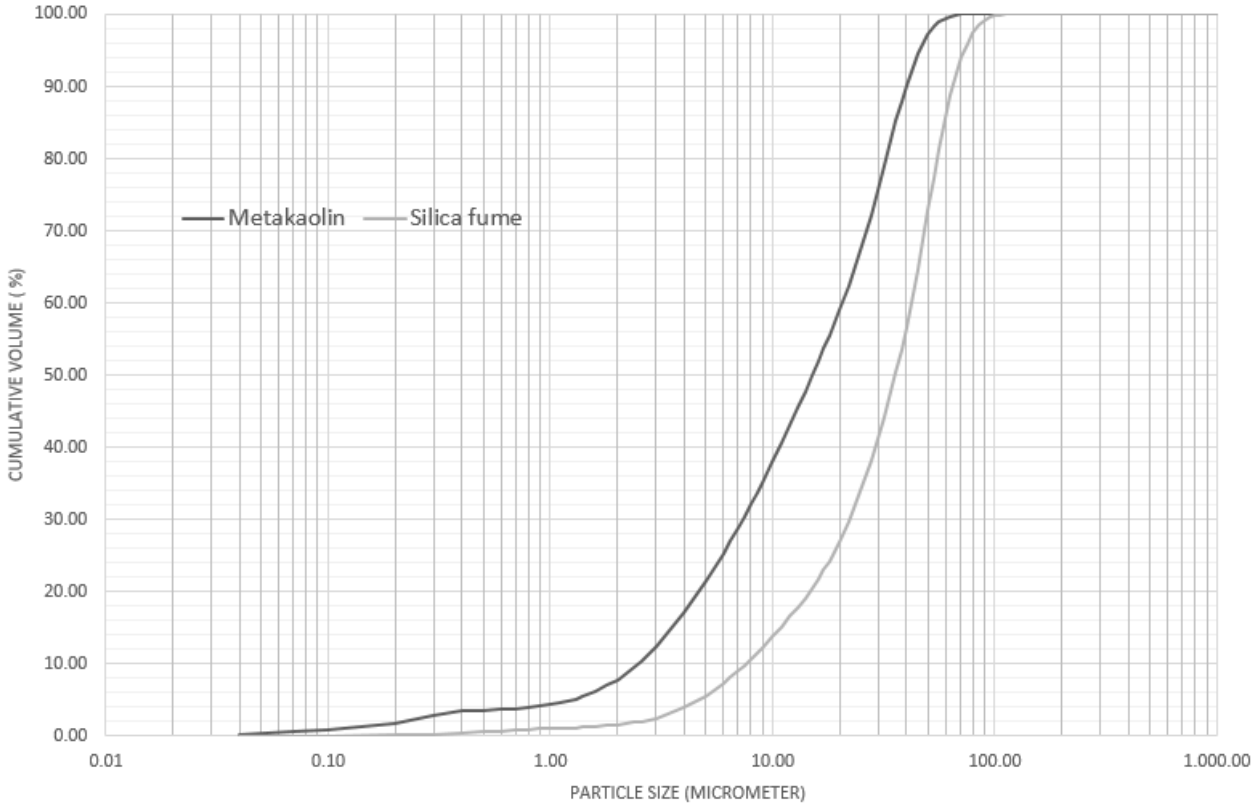

627

628

629 Figure 3

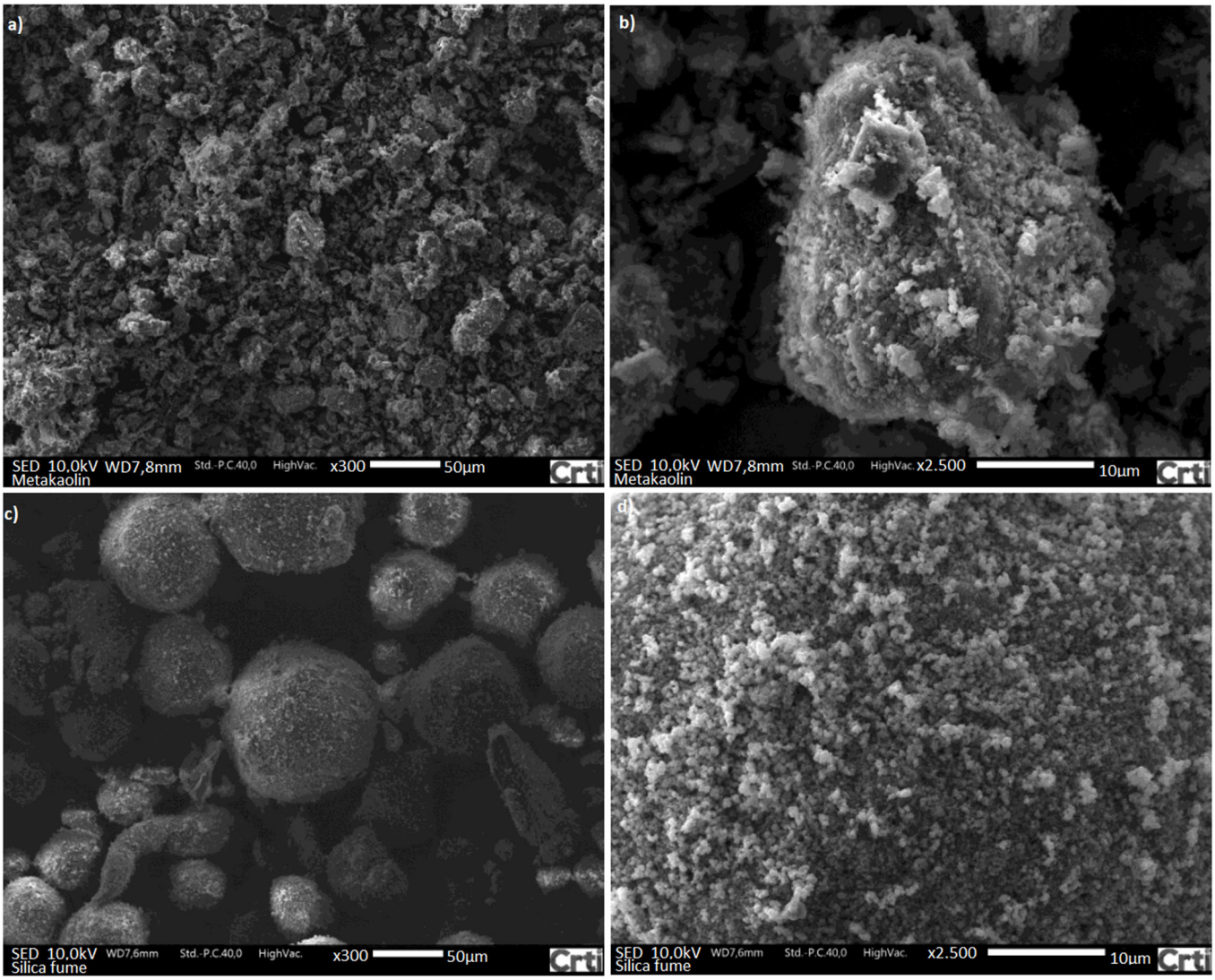

630

631

632 Figure 4

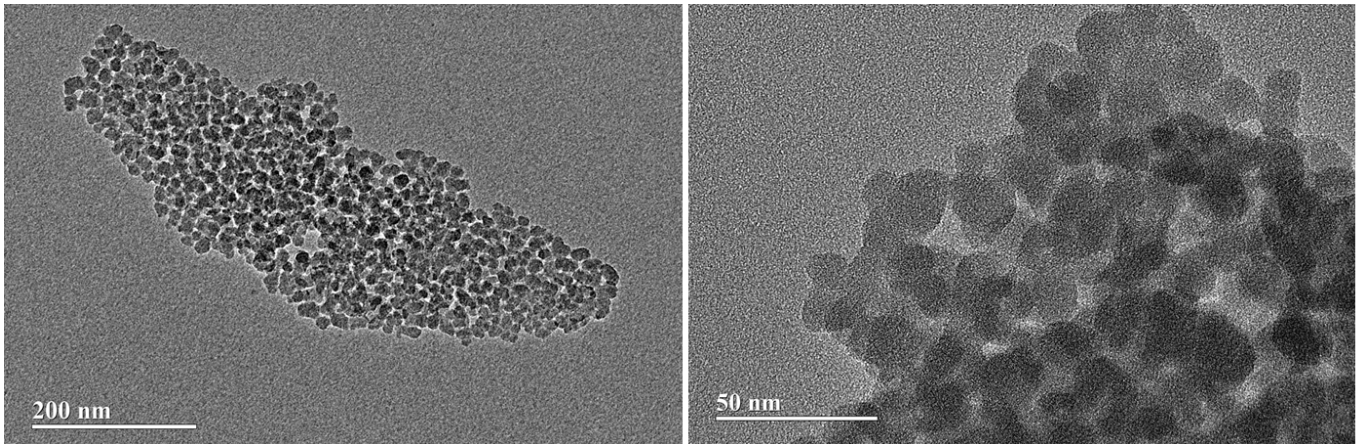

633

634

635 Figure 5

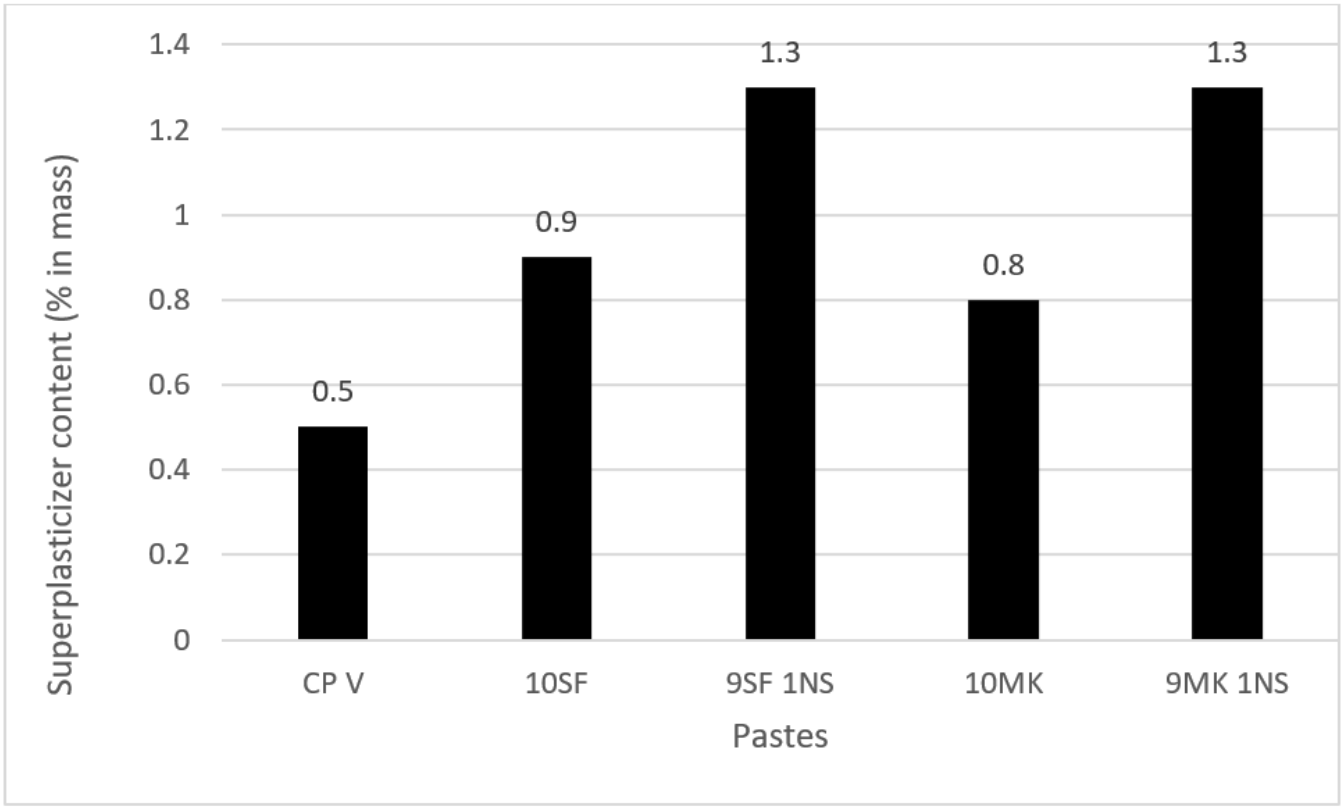

636

637

638 Figure 6

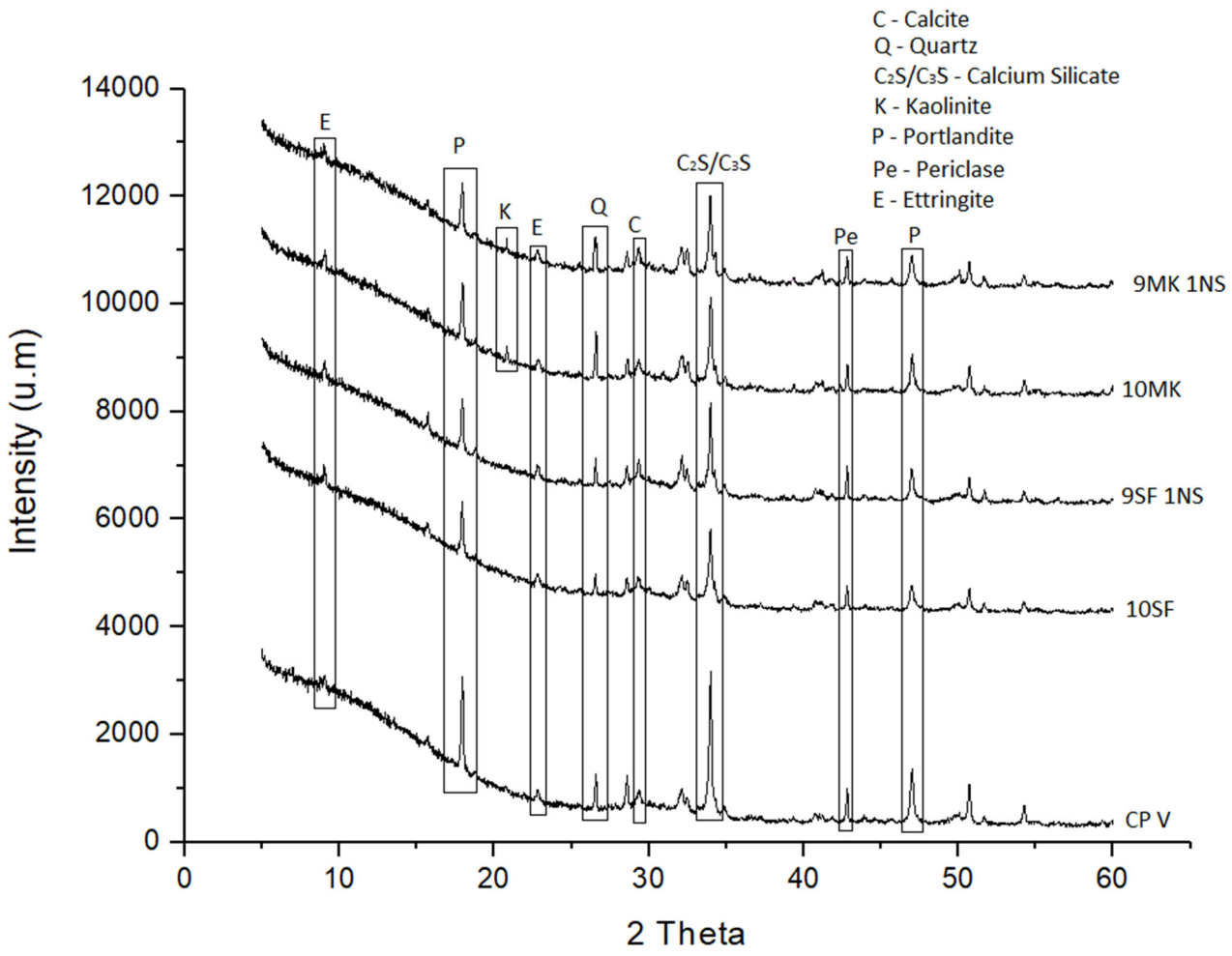

639

640

641 Figure 7

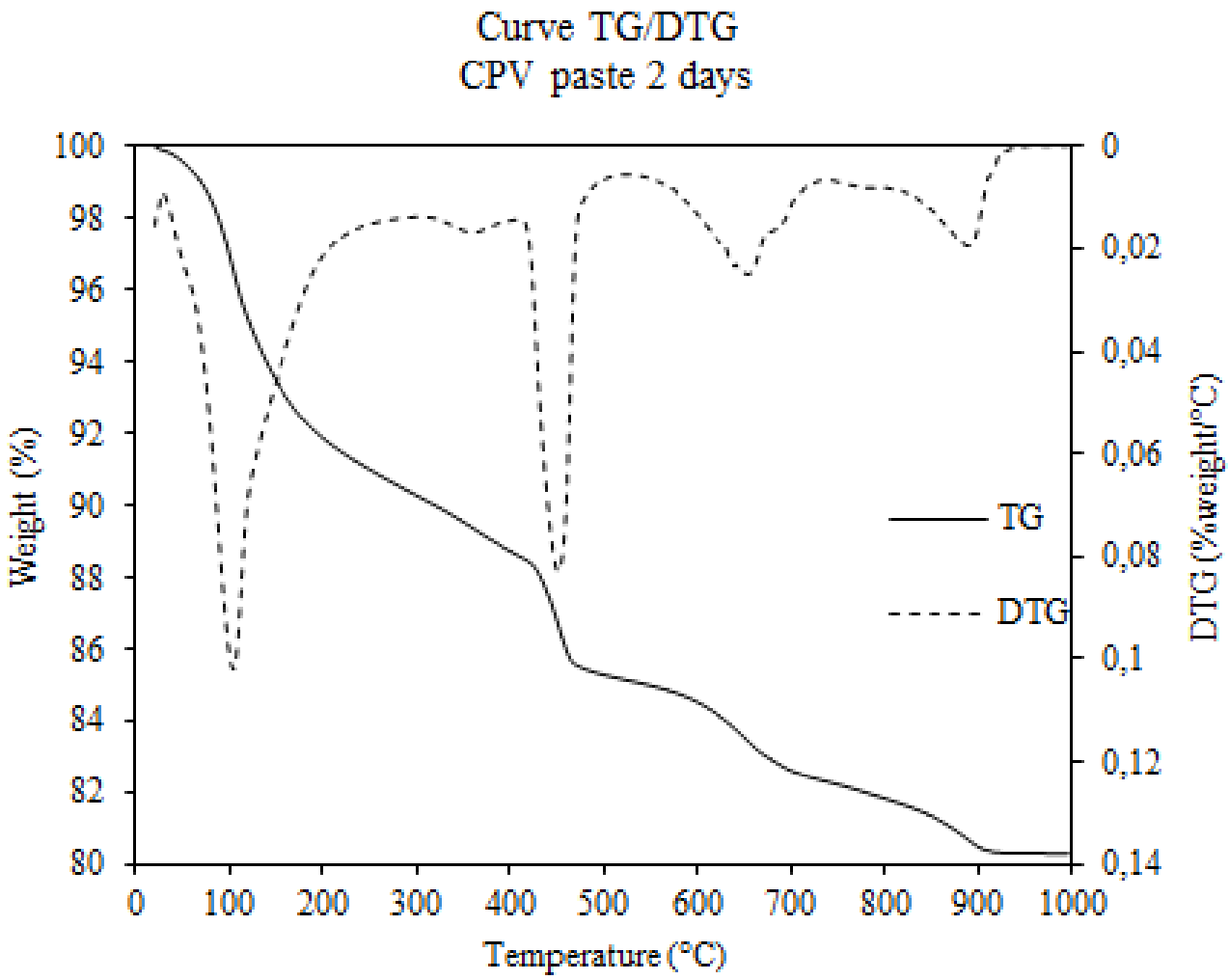

642

643

644 Figure 8

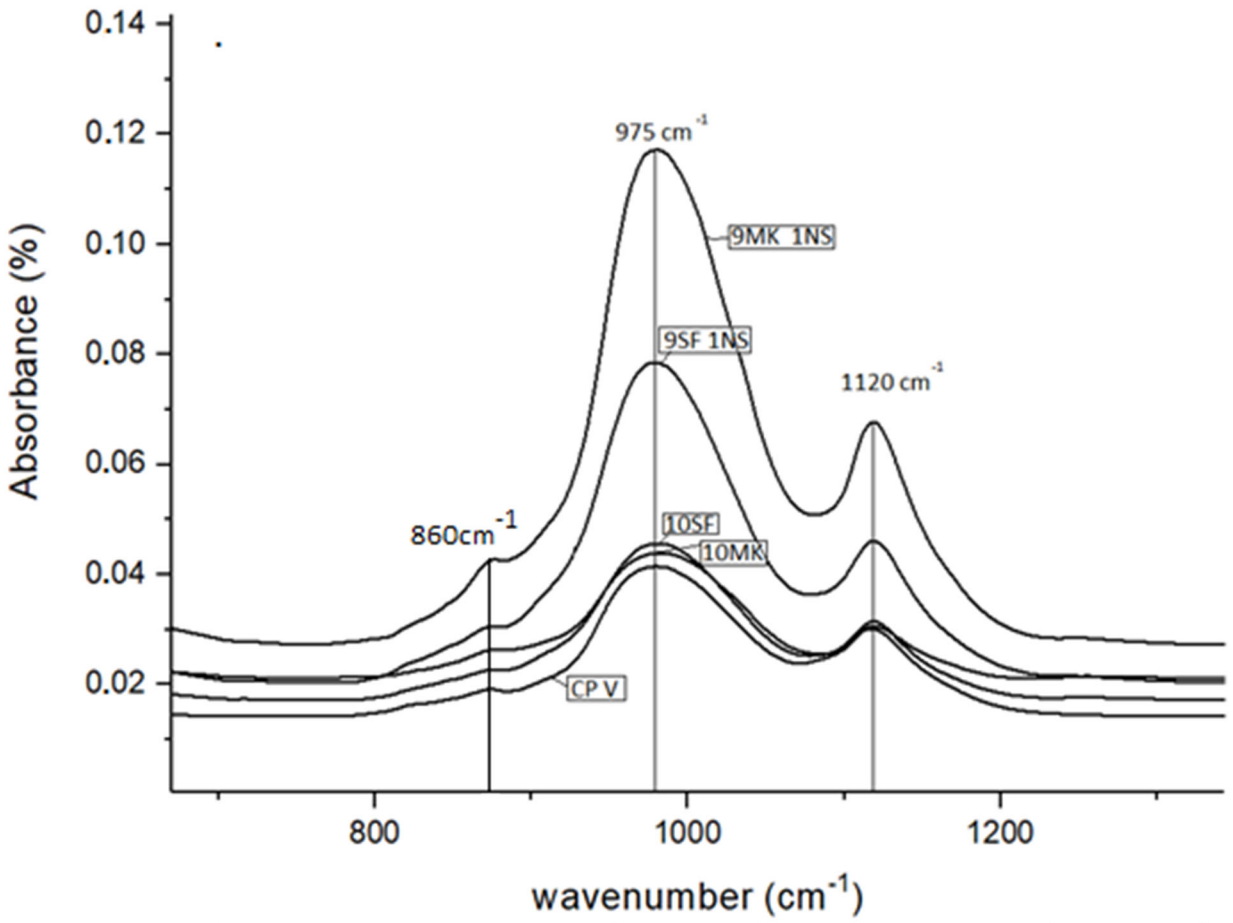

645

646

647 Figure 9

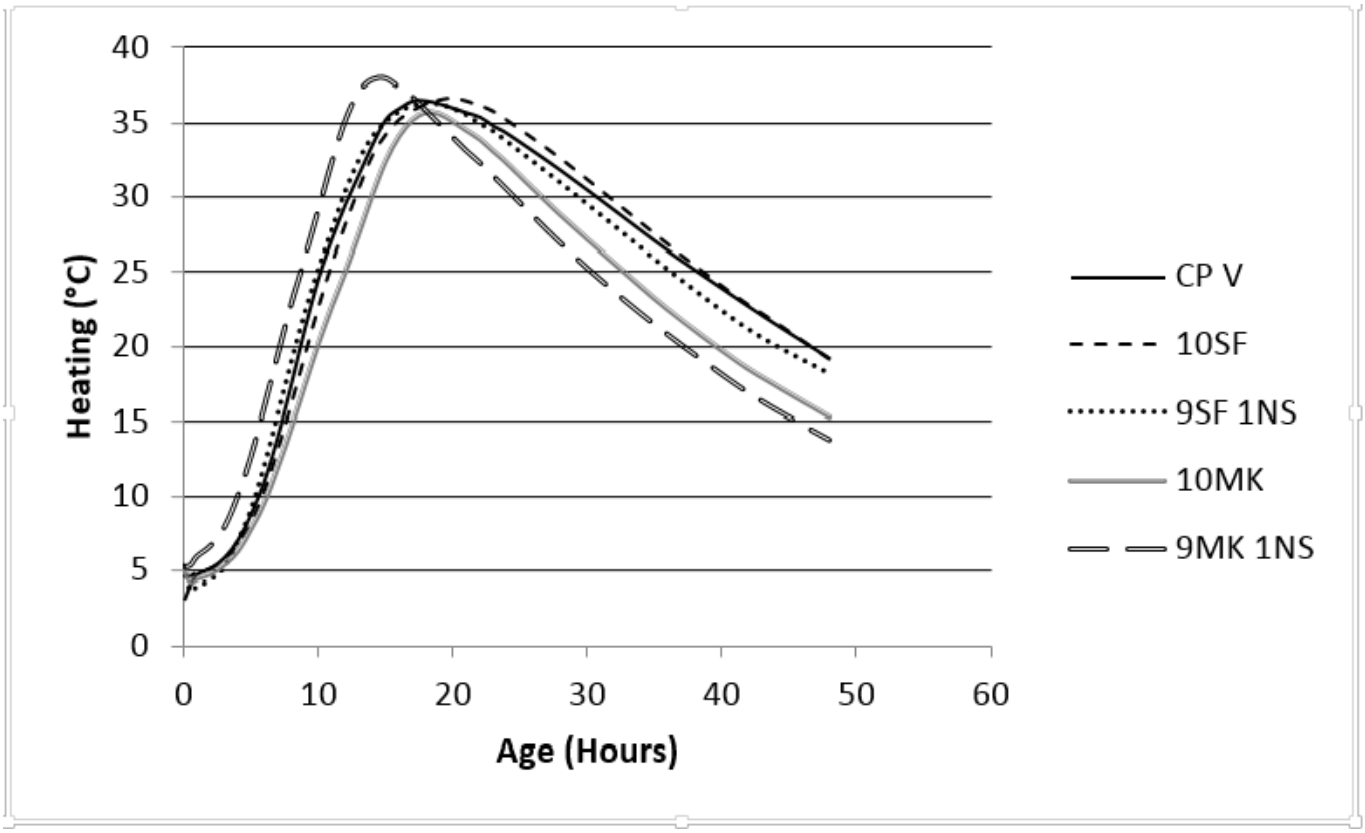

648

649

650 Figure 10

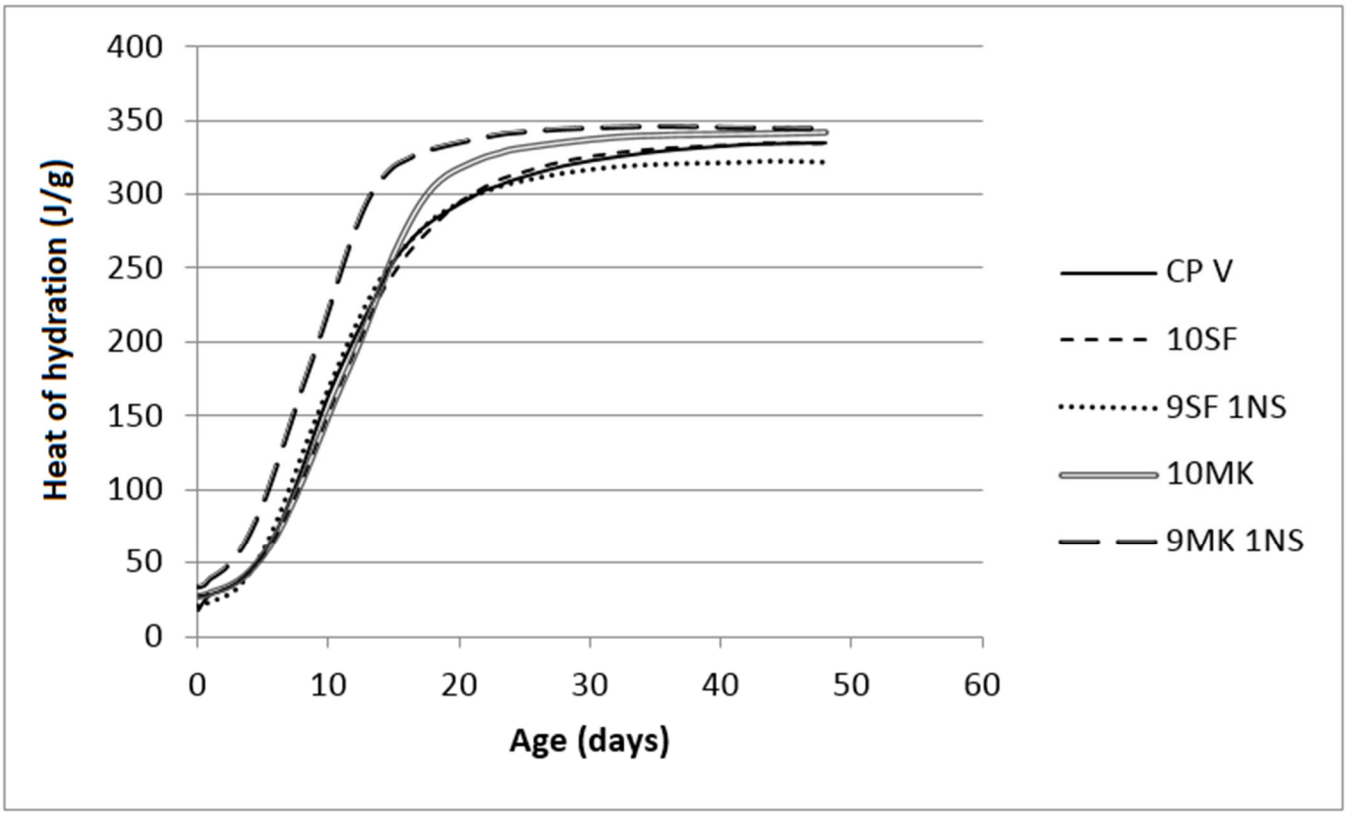

651

652

653 Figure 11

654

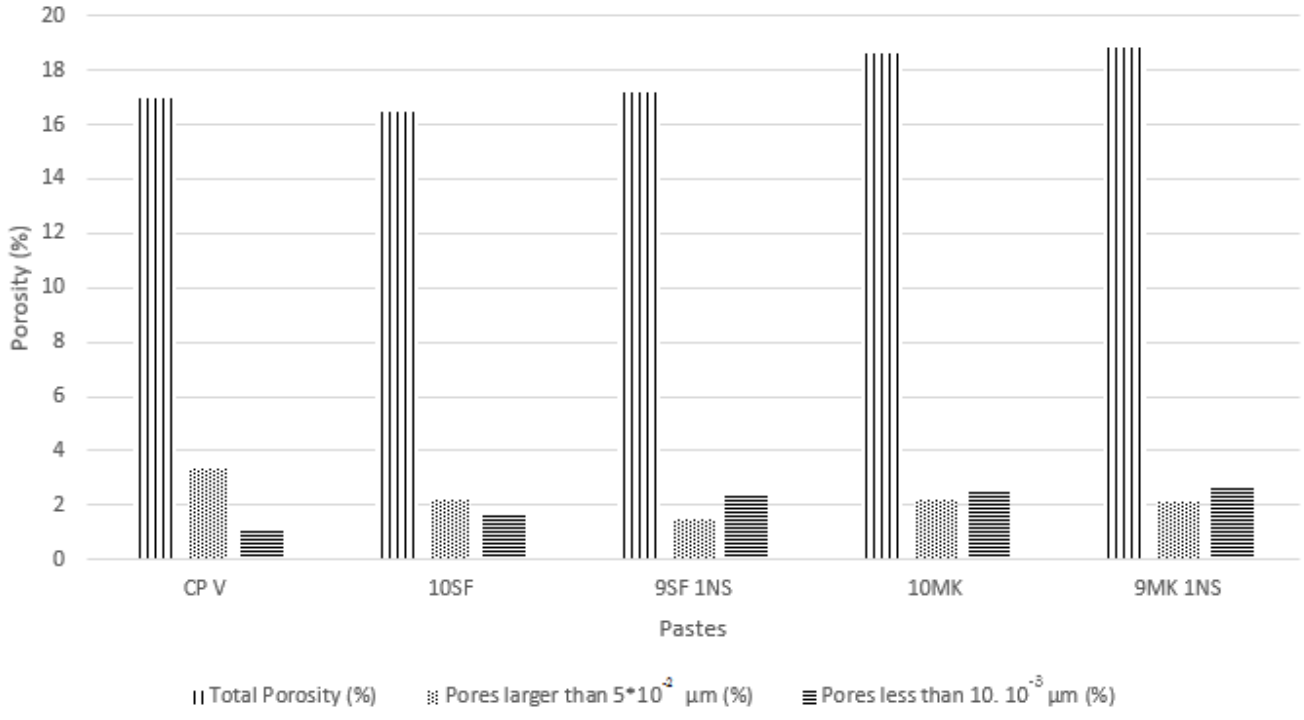

655

656